Available online at www.sciencedirect.com

ScienceDirect

Advances in Space Research 56 (2015) 1538–1545

ADVANCES IN SPACE RESEARCH (a COSPAR publication)

www.elsevier.com/locate/asr

Separation of electrons and protons in the GAMMA-400 gamma-ray telescope

A.A. Leonov [a,*], A.M. Galper [a], V. Bonvicini [b], N.P. Topchiev [c], O. Adriani [d], R.L. Aptekar [e], I.V. Arkhangelskaja [a], A.I. Arkhangelskiy [a], L. Bergstrom [f], E. Berti [d], G. Bigongiari [g], S.G. Bobkov [h], M. Boezio [b], E.A. Bogomolov [e], S. Bonechi [g], M. Bongi [d], S. Bottai [d], G. Castellini [i], P.W. Cattaneo [j], P. Cumani [b], G.L. Dedenko [a], C. De Donato [k], V.A. Dogiel [c], M.S. Gorbunov [h], Yu.V. Gusakov [c], B.I. Hnatyk [l], V.V. Kadilin [a], V.A. Kaplin [a], A.A. Kaplun [a], M.D. Kheymits [a], V.E. Korepanov [m], J. Larsson [n], V.A. Loginov [a], F. Longo [b], P. Maestro [g], P.S. Marrocchesi [g], V.V. Mikhailov [a], E. Mocchiutti [b], A.A. Moiseev [o], N. Mori [d], I.V. Moskalenko [p], P.Yu. Naumov [a], P. Papini [d], M. Pearce [n], P. Picozza [k], A. Rappoldi [j], S. Ricciarini [i], M.F. Runtso [a], F. Ryde [n], O.V. Serdin [h], R. Sparvoli [k], P. Spillantini [d], S.I. Suchkov [c], A.A. Taraskin [a], M. Tavani [q], A. Tiberio [d], E.M. Tyurin [a], M.V. Ulanov [e], A. Vacchi [b], E. Vannuccini [d], G.I. Vasilyev [e], Yu.T. Yurkin [a], N. Zampa [b], V.N. Zirakashvili [r], V.G. Zverev [a]

[a] *National Research Nuclear University "MEPhI", Kashirskoe shosse, 31, Moscow, Russia*
[b] *Istituto Nazionale di Fisica Nucleare, Sezione di Trieste and Physics Department of University of Trieste, Trieste, Italy*
[c] *Lebedev Physical Institute, Russian Academy of Sciences, Leninskij Prospekt, 53, Moscow, Russia*
[d] *Istituto Nazionale di Fisica Nucleare, Sezione di Firenze and Physics Department of University of Florence, Firenze, Italy*
[e] *Ioffe Physical Technical Institute, Russian Academy of Sciences, Polytekhnicheskaya, 26, St Petersburg, Russia*
[f] *Stockholm University, Department of Physics; and the Oskar Klein Centre, AlbaNova University Center, Stockholm, Sweden*
[g] *Department of Physical Sciences, Earth and Environment, University of Siena and Istituto Nazionale di Fisica Nucleare, Sezione di Pisa, Pisa, Italy*
[h] *Scientific Research Institute for System Analysis, Russian Academy of Sciences, Moscow, Russia*
[i] *Istituto di Fisica Applicata Nello Carrara – CNR and Istituto Nazionale di Fisica Nucleare, Sezione di Firenze, Firenze, Italy*
[j] *Istituto Nazionale di Fisica Nucleare, Sezione di Pavia, Pavia, Italy*
[k] *Istituto Nazionale di Fisica Nucleare, Sezione di Roma 2 and Physics Department of University of Rome Tor Vergata, Rome, Italy*
[l] *Taras Shevchenko National University of Kyiv, Kyiv, Ukraine*

* Corresponding author.
E-mail addresses: leon@ibrae.ac.ru (A.A. Leonov), amgalper@mephi.ru (A.M. Galper), Bonvicini@ts.infn.it (V. Bonvicini), tnp51@rambler.ru (N.P. Topchiev), adriani@fi.infn.it (O. Adriaini), aptekar@mail.ioffe.ru (R.L. Aptekar), irene.belousova@usa.net (I.V. Arkhangelskaja), angel1966@list.ru (A.I. Arkhangelskiy), lbe@fysik.su.se (L. Bergstrom), berti@fi.infn.it (E. Berti), gabriele@df.unipi.it (G. Bigongiari), bobkov@cs.niisi.ras.ru (S.G. Bobkov), Mirko.Boezio@trieste.infn.it (M. Boezio), edward.bogomolov@gmail.com (E.A. Bogomolov), lorenzo.bonechi@fi.infn.it (S. Bonechi), bongi@fi.infn.it (M. Bongi), bottai@fi.infn.it (S. Bottai), g.castellini@ifac.cnr.it (G. Castellini), Paolo.Cattaneo@pv.infn.it (P.W. Cattaneo), Paolo.Cumani@ts.infn.it (P. Cumani), gldedenko@mephi.ru (G.L. Dedenko), cinzia.dedonato@roma2.infn.it (C. De Donato), dogiel@lpi.ru (V.A. Dogiel), gorbunov@cs.niisi.ras.ru (M.S. Gorbunov), iourii.goussakov@cern.ch (Y.V. Gusakov), bohdan_hnatyk@ukr.net (B.I. Hnatyk), vvkadilin@mephi.ru (V.V. Kadilin), kaplinv@mail.ru (V.A. Kaplin), akaplun@atsys.ru (A.A. Kaplun), mcsaksik@gmail.com (M.D. Kheymits), vakor@isr.lviv.ua (V.E. Korepanov), jlarsson@particle.kth.se (J. Larsson), vloginov49@mail.ru (V.A. Loginov), francesco.longo@ts.infn.it (F. Longo), paolo.maestro@pi.infn.it (P. Maestro), marrocchesi@pi.infn.it (P.S. Marrocchesi), vvmikhajlov@gmail.com (V.V. Mikhailov), Emiliano.Mocchiutti@ts.infn.it (E. Mocchiutti), amoiseev@astro.umd.edu (A.A. Moiseev), mori@fi.infn.it (N. Mori), imos@stanford.edu (I.V. Moskalenko), pynaumov@mephi.ru (P.Yu. Naumov), papini@fi.infn.it (P. Papini), pearce@kth.se (M. Pearce), piergiorgio.picozza@roma2.infn.it (P. Picozza), Andrea.Rappoldi@pv.infn.it (A. Rappoldi), ricciarini@fi.infn.it (S. Ricciarini), mfruntso@mephi.ru (M.F. Runtso), felix@particle.kth.se (F. Ryde), serdin@cs.niisi.ras.ru (O.V. Serdin), sparvoli@roma2.infn.it (R. Sparvoli), piero.spillantini@fi.infn.it (P. Spillantini), soutch@mail.ru (S.I. Suchkov), antonnidhoggr@me.com (A.A. Taraskin), tavani@iasf-roma.inaf.it (M. Tavani), tiberio@fi.infn.it (A. Tiberio), tempost@mail.ru (E.M. Tyurin), ulanov@mail.ioffe.ru (M.V. Ulanov), Vacchi@trieste.infn.it (A. Vacchi), vannucci@fi.infn.it (E. Vannuccini), gennady.vasilyev@mail.ioffe.ru (G.I. Vasilyev), YTYurkin@mephi.ru (Y.T. Yurkin), Nicola.Zampa@ts.infn.it (N. Zampa), zirak@izmiran.ru (V.N. Zirakashvili), zverev@x4u.lebedev.ru (V.G. Zverev).

http://dx.doi.org/10.1016/j.asr.2015.06.040

[m] Lviv Center of Institute of Space Research, Lviv, Ukraine
[n] KTH Royal Institute of Technology, Department of Physics; and the Oskar Klein Centre, AlbaNova University Center, Stockholm, Sweden
[o] CRESST/GSFC and University of Maryland, College Park, MA, USA
[p] Hansen Experimental Physics Laboratory and Kavli Institute for Particle Astrophysics and Cosmology, Stanford University, Stanford, USA
[q] Istituto Nazionale di Astrofisica IASF and Physics Department of University of Rome Tor Vergata, Rome, Italy
[r] Pushkov Institute of Terrestrial Magnetism, Ionosphere, and Radiowave Propagation, Troitsk, Moscow Region, Russia

Received 13 October 2014; received in revised form 23 June 2015; accepted 25 June 2015
Available online 6 July 2015

Abstract

The GAMMA-400 telescope will measure the fluxes of gamma rays and cosmic-ray electrons and positrons in the energy range from 100 MeV to several TeV. These measurements will allow it to achieve the following scientific objectives: search for signatures of dark matter, investigation of gamma-ray point-like and extended sources, study of the energy spectrum of the Galactic and extragalactic diffuse emission, study of gamma-ray bursts and gamma-ray emission from the active Sun, together with high-precision measurements of the high-energy electrons and positrons spectra, protons and nuclei up to the knee.

The bulk of cosmic rays are protons and helium nuclei, whereas the lepton component in the total flux is $\sim 10^{-3}$ at high energy. In the present paper, the simulated capability of the GAMMA-400 telescope to distinguish electrons and positrons from protons in cosmic rays is addressed. The individual contribution to the proton rejection from each detector system of GAMMA-400 is studied separately. The use of the combined information from all detectors allows us to reach a proton rejection of the order of $\sim 4 \times 10^5$ for vertical incident particles and $\sim 3 \times 10^5$ for particles with initial inclination of 30° in the electron energy range from 50 GeV to 1 TeV.

Keywords: Gamma-ray telescope; Hadron and electromagnetic showers; Gamma rays; Cosmic rays; Space experiments

1. Introduction

The GAMMA-400 instrument was developed to address a broad range of scientific goals, such as search for signatures of dark matter, studies of galactic and extragalactic gamma-ray sources, galactic and extragalactic diffuse emission, gamma-ray bursts, as well as high-precision measurements of spectra of cosmic-ray electrons, positrons, and nuclei (Galper et al., 2013). In this paper, electron and proton separation methods for GAMMA-400 are presented.

Instruments used in satellite-borne experiments and devoted to the study of high-energy cosmic rays need to identify the incoming particles and measure their energies. This identification is usually based on the analysis of the longitudinal and transversal shower profiles and the total energy deposition in a calorimetric system; in particular, in order to separate the electromagnetic from the hadronic component, it is possible to take into account that these two showers have different spatial and energy topology forms (Fabjan and Gianotti, 2003). Moreover, the number of neutrons generated in the electromagnetic cascade is much less than that in the hadronic cascade; the neutron detection significantly improves the separation of electrons from protons (Adriani et al., 2009; Stozhkov et al., 2005). The combined information from all detector systems provides a proton rejection factor for vertical and inclined protons better than 10^5, which is the level needed to recognize electrons over a background of protons.

2. The detector systems of the GAMMA-400 gamma-ray telescope

The GAMMA-400 physical scheme is shown in Fig. 1. GAMMA-400 consists of scintillation anticoincidence top and lateral detectors (AC top and AC lat), a converter-tracker (C) with 8 layers of double (x, y) silicon strip coordinate detectors (pitch of 0.1 mm) interleaved with tungsten conversion foils and 2 layers of double (x, y) silicon strip coordinate detectors without tungsten at the bottom, 2 scintillation detectors (S1 and S2) for the Time-of-Flight system (ToF), a calorimeter made of 2 parts (CC1 and CC2), lateral detectors (LD), scintillation detectors (S3 and S4) and neutron detector (ND).

The anticoincidence detectors surrounding the converter-tracker serve to distinguish gamma-ray events from the much more numerous charged-particle events. Converter-tracker information is applied to precisely determine the direction of each incident particle and the calorimeter measurements are used to determine its energy. The Time-of-Flight system, where detectors S1 and S2 are separated by 500 mm, distinguishes the upward or downward direction of the arriving particle. Additional scintillation detectors S3 and S4 improve the separation of electromagnetic and hadronic showers. All scintillation detectors consist of 2 independent layers, each one with a thickness of 1 cm.

The imaging calorimeter CC1 consists of 2 layers of double (x, y) silicon strip coordinate detectors (pitch of

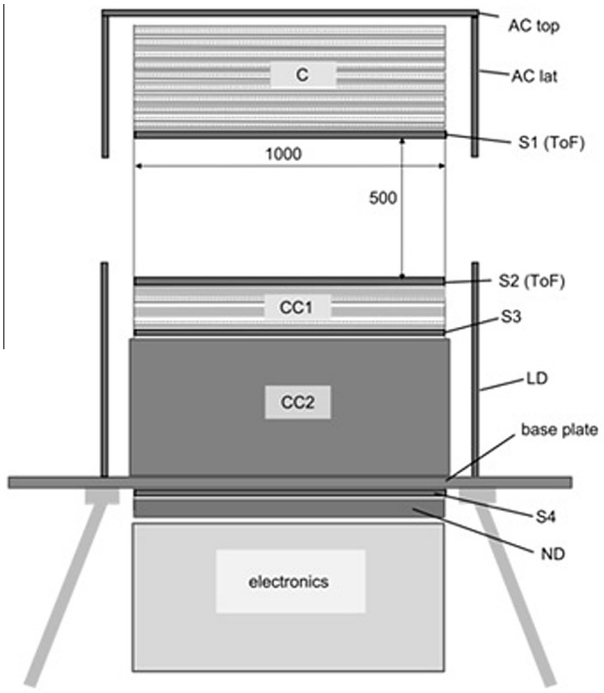

Fig. 1. GAMMA-400 physical scheme. AC top is the top anticoincidence detector, AC lat are lateral anticoincidence detectors, C is the converter-tracker; S1 (ToF) and S2 (ToF) are scintillation detectors of the Time-of-Flight system, CC1 and CC2 are coordinate-sensitive and electromagnetic calorimeter, S3 and S4 are scintillation detectors, ND is the neutron detector.

0.1 mm) interleaved with planes from CsI(Tl) crystals, and the electromagnetic calorimeter CC2 consists of CsI(Tl) crystals with the dimensions of 36 mm × 36 mm × 430 mm. The long axis of these crystals is "vertical" (parallel to the axis of the instrument). The total converter-tracker thickness is about 1 radiation length X_0. The thicknesses of CC1 and CC2 are 2 X_0 and 23 X_0, respectively. The total calorimeter thickness is 25 X_0 or 1.2 nuclear interaction lengths λ_0. Using a thick calorimeter allows us to extend the energy range up to several TeV and reach an energy resolution better than 1% for electrons above 100 GeV.

3. Methods to reject protons from electrons in GAMMA-400

Protons are the main background when detecting cosmic-ray electrons, since the fraction of the lepton component is $\sim 10^{-3}$ of the total cosmic-ray flux at high energies. Simulations of the rejection factor of protons from electrons in GAMMA-400 were performed with the Geant4 simulation toolkit software (http://geant4.cern.ch).

To reject protons from electrons, information from ND, S4, S3, S2, CC1, and CC2 is used. Every detector is considered as a "separate layer of a composite calorimeter", and the ability of each layer to decrease the proton contamination in the different energy region is investigated individually. In principle, an interacting proton with energy more than 100 GeV could imitate a 100 GeV electron, since it can release the same energy deposit in the GAMMA-400 calorimeter. The rejection factor at 100 GeV is then calculated as the ratio of the number of initial protons with energy more than 100 GeV – assuming that the proton energy spectrum power-index is −2.7 – to the number of events identified as electrons with energy 100 ± 2 GeV (taking into account that the GAMMA-400 energy resolution is equal to about 2%). This approach is specific for the instrument configuration, considering the total depth of the materials (∼1.2 λ_0) – which defines the probability of proton nuclear interactions inside the calorimeter – the mean energy of protons that might mimic 100 GeV electrons and the energy resolution. The intrinsic rejection of GAMMA-400 is due to its interaction depth and the energy resolution is implicitly contributed in the analysis for each layer of the composite calorimeter.

Analysis of electron measurements and proton rejection techniques using calorimeters that nearly fully contain electromagnetic showers but are thin in hadronic interaction lengths – as the GAMMA-400 calorimeter is – have been carried out many times. These have consistently indicated that the most powerful physical observables to separate an electromagnetic from a hadronic shower are the initial point of the shower, the lateral distribution of particles in the calorimeter and the longitudinal shower development. Taking into account the GAMMA-400 instrument structure, the information from CC2 can be used for reconstructing the lateral distribution of particles in the shower; the S4 response can be used to reduce the proton contamination from the longitudinal shower development. The initial point of the shower is reconstructed by the information of S2, S3, and CC1 detectors. The information from the neutron detector also improves the separation of electrons from protons, especially for energy greater than 50 GeV (Stozhkov et al., 2005).

In our analysis, we first evaluated the contamination for vertical incident protons. All processed criteria to suppress protons are based on selecting cutoffs to distinguish proton and electron events. Such cutoffs are determined in such a way to retain 98% of electrons. In total, 25 cutoffs are used to reject protons. Taking into account this selection, roughly 30% of electrons are also lost due to proton rejection. The list of the criteria is ordered according to their intrinsic rejection power. Regarding the data of the Neutron Detector, since its efficiency will be the object of a future more detailed calculation, the power of the ND criterion can be considered as upper estimation of its own rejection.

For a correct calculation of the intrinsic rejection in scintillation counters, the width of the distribution of the signal amplitudes for electrons and protons is the most important parameter. In Geant 4 simulations, the value of the scintillation detector response is formed only by ionization losses of the particle inside the detector. To take into account the efficiency of the released energy conversion into the light flash, the efficiency of light collection

and the efficiency of the light to electric signal transformation in a photomultiplier, data from a beam test calibration were used (Boezio et al., 2004). In Fig. 2, the solid line represents the dependence of the ratio of RMS to the mean signal in scintillation detector as a function of the electron energy in the CERN calibration test beam. This calibration was performed in the frame of PAMELA experiment for scintillation detectors similar to the ones that will be used in the GAMMA-400 instrument. The Geant4 simulation results are also shown in Fig. 2 by the dashed line. Comparing the results of calibration and simulation, it is possible to introduce an additional spreading parameter for the simulated data. The value of a signal in the scintillation detector is calculated as:

$$E = E_0 + E',$$

where E_0 is the energy release due to ionization losses, E' is the spreading signal calculated from the Gauss distribution with $\sigma \approx 0.33 \times E_0 - 4 \times (10^{-4}) \times E_0^2$, E_0 is determined in MIPs (MIP is minimum ionizing particle, 1 MIP is equal to $\sim$ 2 MeV for S4).

Such spreading of the simulated response was applied to all scintillation detectors: S2, S3, and S4. The information from S4 – located at the bottom of the calorimeter – provides the strongest intrinsic rejection factor for protons; this fact is due to the difference in attenuation for hadronic and electromagnetic cascades. Electromagnetic shower initiated by an electron with initial energy of $\sim$100 GeV is fully contained inside a calorimeter with the thickness 25 X_0 or 1.2 λ_0. Such criterion was used in the PAMELA experiment data analysis (Karelin et al., 2013). The distributions of signals in S4 from incoming electrons and protons are shown in Fig. 3(a) and (c). By selecting events with signals in S4 less than 2.7 MIP, it is possible to suppress protons with a factor of 100.

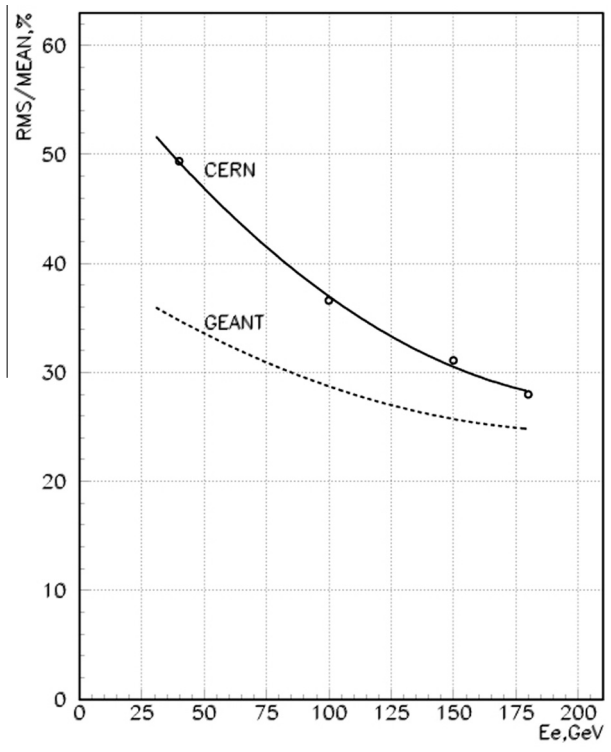

Fig. 2. Dependence of the ratio of RMS to the average signal in scintillation detector as a function of the electron energy in the CERN calibration test beam (solid line); the same distribution for simulated data (dashed line).

Additional rejection is obtained when analyzing the total CC2 signals. The CC2 calorimeter contains CsI(Tl) square crystals with cross dimension of 36 mm and longitudinal dimension of 430 mm. The criterion is based on the difference of the transversal size for hadronic and electromagnetic showers. Such a topology difference was successfully applied with the calorimeter data in the PAMELA mission to separate electrons from an antiproton sample and positrons from a proton sample (Karelin et al., 2013; Menn et al., 2013). In Fig. 3(b) and (d) the distributions of the ratio between a signal in the crystal containing the axis cascade and the value of the total signal in CC2 for incoming electrons and protons are compared. Using the distribution for the electrons, two cut-off values are determined: 71.3% and 74.4%. For the proton distribution, only events placed between these electron cutoffs are retained. Applying this criterion, a rejection factor of $\sim$30 is obtained.

The differences in the proton and electron cascade transverse size are also used when analyzing information from silicon strips in CC1. The distributions for RMS of coordinates of strips with signals for incoming electrons and protons are shown in Fig. 4(a) and (b). For the proton distribution, only events placed between the cutoffs of 0.3 cm and 8 cm obtained by the electron distribution are retained. The application of this criterion provides a rejection factor of $\sim$6.

To take into account the fact that the hadronic cascade begins to develop deeper inside the instrument than the electromagnetic one, the signals in CC1 (crystal), S2 and S3 are considered, using the fact that the thickness of material just above these detectors is less than 4 X_0. The distributions of signals in the second layer of crystal CsI(Tl) from CC1 and of signals in S3 from electrons and protons are shown in Fig. 5. For proton-induced cascades, there are a lot of events with small signal amplitude. To reject such events, a cutoff from the electron induced cascade distribution is determined. This criterion allows us to suppress protons with a factor 3 for each CsI(Tl) crystal of CC1 and with a factor 2 for each scintillation detector S2 and S3.

The ND contribution in the rejection factor for protons in the GAMMA-400 telescope is due to the fact that in cascades induced by protons the generation of neutrons is more intensive than in the electromagnetic ones. The source of neutrons in cascades induced by electrons is due mainly to the generation of gamma rays in those cascades with energy close to 17 MeV. These gamma rays, in turn, could generate neutrons in the Giant resonance reaction.

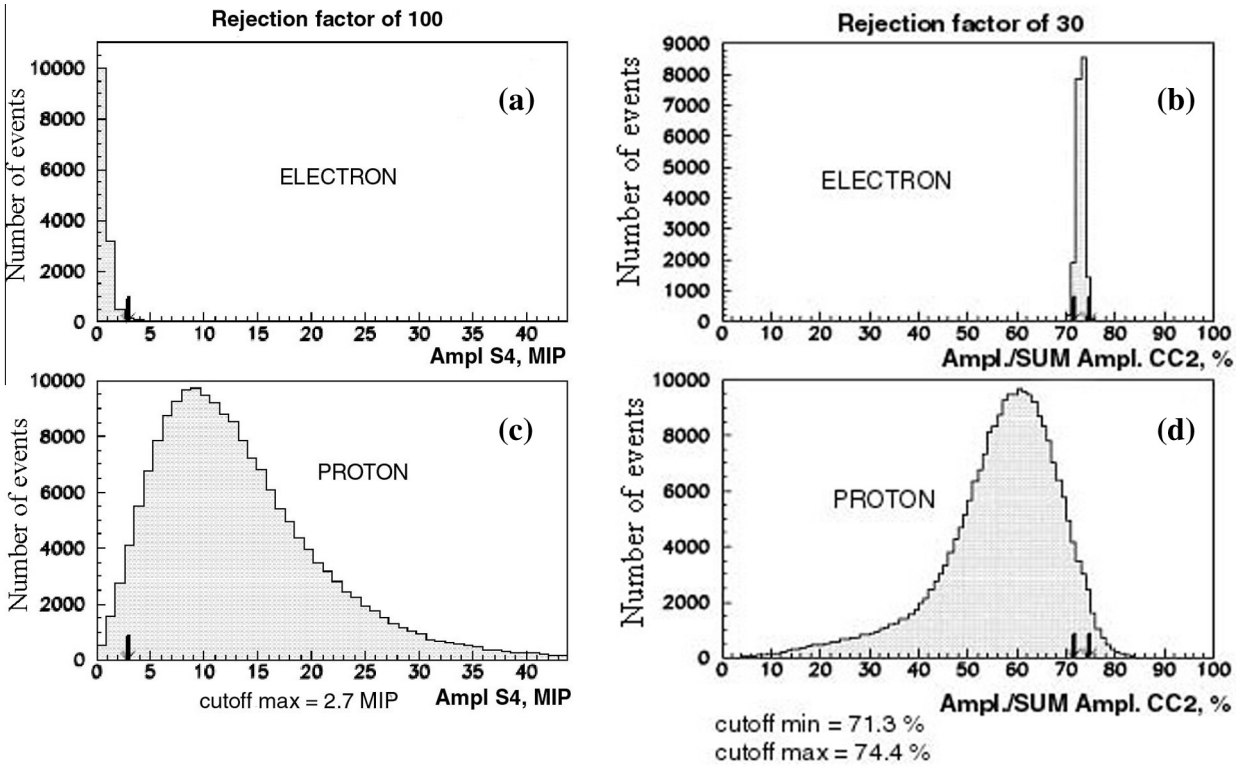

Fig. 3. Distributions for signals in S4 from electrons (a) and protons (c); Distributions for the ratio of a signal in the crystal containing the cascade axis to the value of total signal in CC2 for electrons (b) and protons (d).

Analyzing information from the neutron detector placed just under the CC2 calorimeter, it may be possible to suppress protons by a factor 400. The distributions of the number of neutrons at the entrance of ND from incoming electrons and protons are shown in Fig. 6. A cutoff for the number of neutrons to separate protons is set to 60. The efficiency of neutron detection is not taken into account in the present simulation, but will be the purpose of a future more detailed calculation. The power of this criterion can be considered as an upper estimation of ND intrinsic rejection.

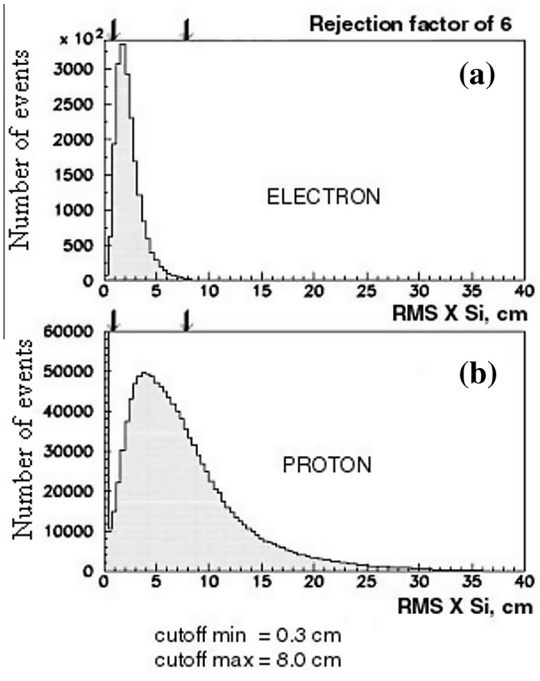

Fig. 4. Distributions for RMS of coordinates of strips with signals in CC1 for electrons (a) and protons (b).

All proton rejection criteria of the single detectors, discussed above, were considered individually. Using all criteria in cascade, it is possible to obtain a rejection factor for protons equal to $(4 \pm 0.4) \times 10^5$. Table 1 contains the information about intrinsic rejection factors of each detector individually, and the decrease of the total rejection factor in the case of neglecting that specific detector. All criteria are strongly dependent from each other, and that is confirmed by the values in the most right column. The elimination of a single detector from the full criterion cascade, especially the most powerful S4, CC2 and CC1 detectors, reduces the total rejection factor significantly less than dividing the total value of the proton rejection factor by the intrinsic detector one.

The same proton rejection algorithm was applied for inclined incident protons. The values of the cutoffs for the rejection procedure of course change: to suppress inclined protons, only events with a number of neutrons in ND less than 75 are retained; to reject inclined protons, only events with signals in S4 less than 1.1 MIP are considered.

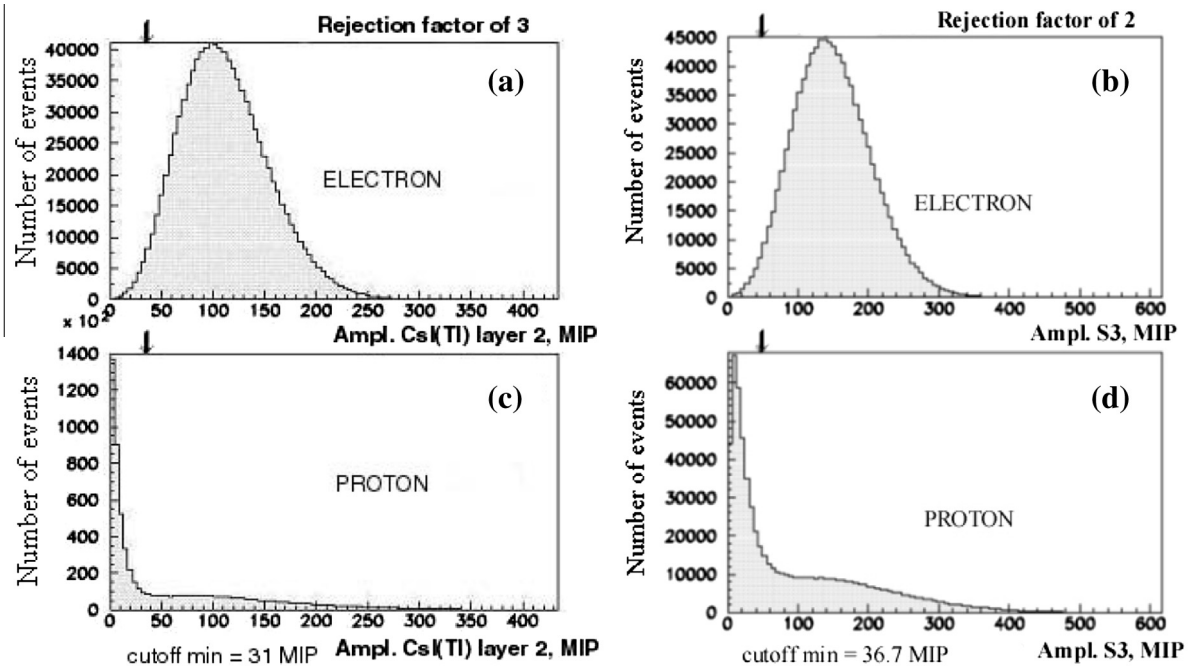

Fig. 5. Distributions of signals in second crystal CsI(Tl) of CC1 for electrons (a) and protons (c); Distributions of signals in S3 for electrons (b) and protons (d).

In CC2, the cascade axis from initial inclined particle crosses mainly three columns of CsI(Tl) crystals. The location of the axis of the cascade in CC2 is presented in Fig. 7. The transverse coordinates of lateral columns from the CsI(Tl) crystal, the column height and transverse coordinates of the cascade axis are also shown. For cascades induced by inclined electrons, the column number 4 (Fig. 7) with the maximum energy release contains only 30% of total energy deposited in CC2 (Fig. 8) instead of 70% for vertical particles (Fig. 3(b) and (d)). Using only distributions for the ratio of the signal in the crystal with maximum energy release to the value of total signal in CC2, it is possible to obtain a rejection factor for inclined protons not greater than 14, instead of 30 for vertical particles. The corresponding cutoffs are 22.2% and 35.0%. But taking into account the distributions in the two other columns (Fig. 9(a) and (c) with cutoffs of 7.7% and 25.8%, Fig. 9(b) and (d) with cutoffs 13.5% and 27.2%), the value of the rejection factor for protons can be increased to 28.

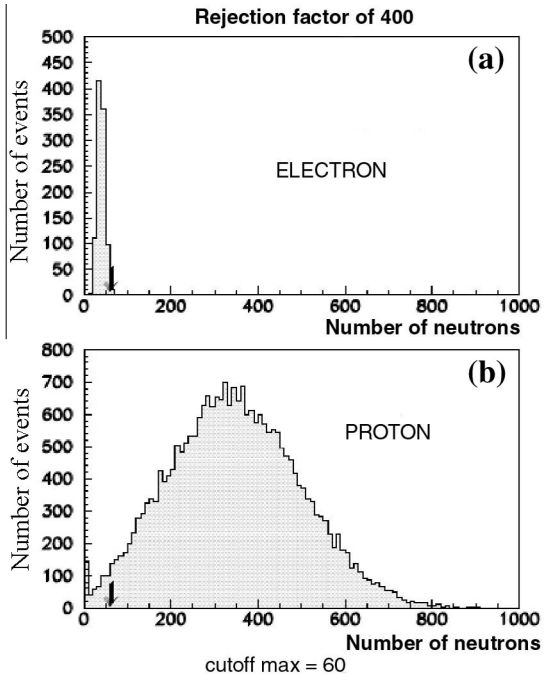

Fig. 6. Distributions of the number of neutrons at the entrance of ND for electrons (a) and protons (b).

Table 1
Intrinsic proton rejection factor for each detector taken individually, and the value of the decrease of the total rejection factor in case of elimination of a given detector from the analysis.

Detector, number of cutoffs	Intrinsic rejection factor	Decrease of the total rejection factor
S4 (2 cutoffs: 1 cutoff for each scintillation layer)	100	1.7
CC2 (2 cutoffs)	30	2.6
Strips in CC1 (4 cutoffs: 2 cutoffs for each X or Y silicon strip)	6	1.2
CsI(Tl) from CC1 (2 cutoffs: 1 cutoff for each layer of CsI(Tl) crystal)	3	1.3
S2, S3 (4 cutoffs: 2 cutoffs for each detector)	2	1.3
ND (1 cutoff)	400 (upper limit)	2

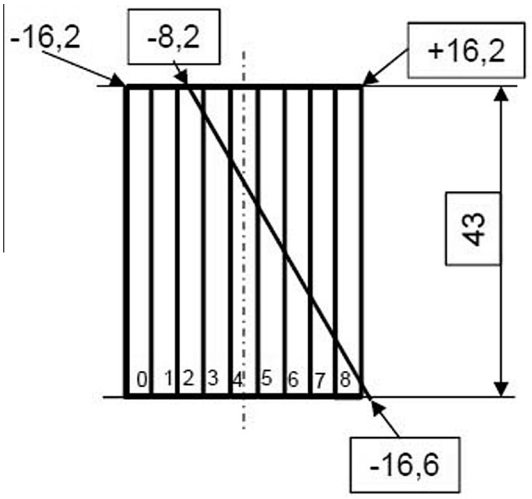

Fig. 7. Location of the axis of the proton induced cascade in CC2 (sloping line). The transverse coordinates of lateral columns from CsI(Tl) crystal, the column height and transverse coordinates of the cascade axis are shown.

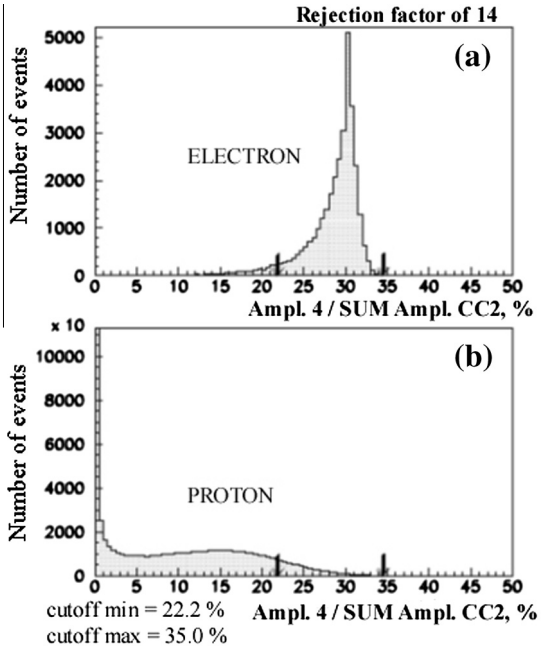

Fig. 8. Distributions for the ratio of signal in the crystal containing the cascade axis with maximum energy release to the value of total signal in CC2 for inclined incident electrons (a) and protons (b).

From the distribution for RMS of coordinates of strips with signals in CC1 for initial inclined electrons, cutoff values of 0.7 cm and 7.4 cm are obtained. New rejection cutoffs for inclined particles for each layer of the CsI(Tl) crystal from CC1, for scintillation detectors S2 and S3 will be 16.4 MIP, 53.3 MIP, 3.5 MIP, and 65.2 MIP, respectively. Using all criteria in the combination, it is possible to obtain a rejection factor for protons with initial incident angle of 30° equal to $(3 \pm 0.4) \times 10^5$.

All these calculations were performed in the energy range from 50 GeV to 1 TeV, in 4 different energy regions. Table 2 contains the information concerning the rejection factors in these bands. The absolute values of all described cutoffs are increased with the gamma-ray initial energy. As

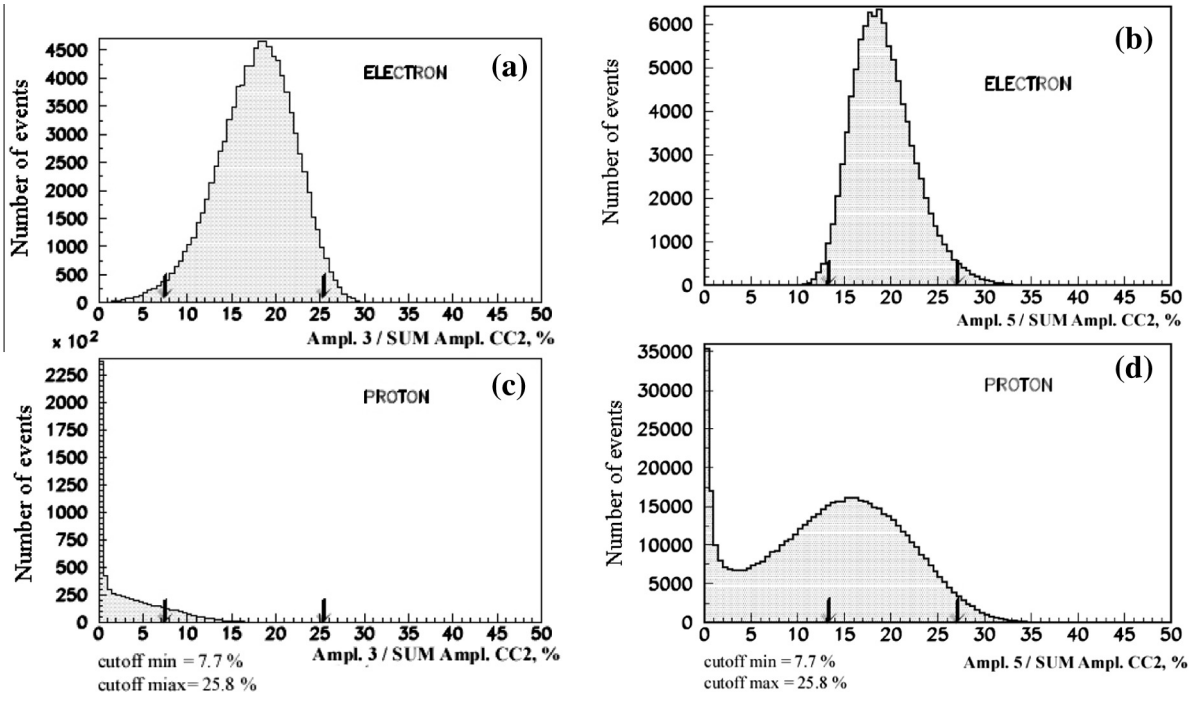

Fig. 9. Distributions for the ratio of signal in the crystal no. 3 from Fig. 7 to the value of total signal in CC2 for initial top-down electrons (a) and top-down protons (c); Distributions for the ratio of signal in the crystal no. 5 from Fig. 7 to the value of total signal in CC2 for initial top-down electrons (b) and top-down protons (d).

Table 2
Total rejection factor to separate protons from electrons in energy range from 50 GeV to 1 TeV.

Energy, GeV	Total rejection factor
50	$(12.8 \pm 2) \times 10^5$
100	$(4.0 \pm 0.4) \times 10^5$
200	$(5.0 \pm 0.7) \times 10^5$
1000	$(4.1 \pm 0.7) \times 10^5$

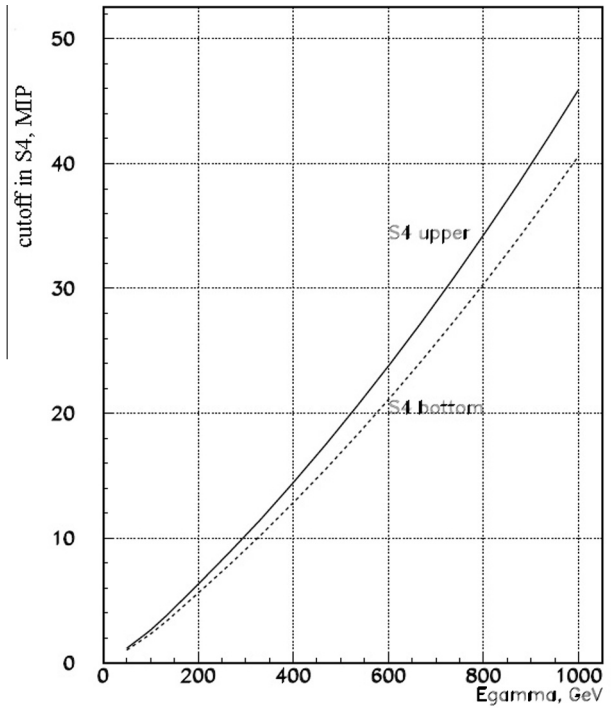

Fig. 10. Dependence of the cutoffs in upper (solid line) and bottom (dotted line) layers of the S4 detector versus the gamma-ray initial energy.

an example, the dependence of the cutoffs in upper and bottom layers of the S4 detector versus the gamma-ray initial energy is presented in Fig. 10. The value of the cutoff in MIPs for the each energy is selected in order to retain 98% of electrons (Fig. 3(a) and (c)).

The own power of the rejection methods was also evaluated as the ratio of the number of initial protons with energy more than 100 GeV – assuming that the proton energy spectrum power-index is −2.7 – depositing 100 ± 2 GeV inside the composite calorimeter to the number of events surviving after the rejection method is applied. This value is equal to $(9 \pm 1) \times 10^3$.

4. Conclusion

Using the combined information from all detector systems of the GAMMA-400 gamma-ray telescope, it is possible to reach an effective rejection of protons from electrons. The methods to separate electron from protons presented in this article are based on the difference of the development of hadronic and electromagnetic showers inside the instrument. It was shown that the rejection factor for vertical and inclined protons is about 5×10^5. Such kind of separation extends in the energy range from 50 GeV to 1 TeV.

References

Adriani, O., Barbarino, G.C., Bazilevskaya, G.A., et al., 2009. An anomalous positron abundance in cosmic rays with energies 1.5–100 GeV. Nature Lett. 458/2, 607–609.

Boezio, M., Bonvicini, V., Mocchiutti, E., et al., 2004. The space experiment PAMELA. Nucl. Phys. B (Proc. Suppl.) 134, 39–46.

Fabjan, C.W., Gianotti, F., 2003. Calorimetry for particle physics. Rev. Mod. Phys. 75, 1243–1286, CERN-EP-2003-075.

Galper, A.M., Adriani, O., Aptekar, R.L., et al., 2013. Status of the GAMMA-400 project. Adv. Space Res. 51, 297–300.

Karelin, A.V., Borisov, S.V., Voronov, S.A., Malakhov, V.V., 2013. Separation of the electron and proton cosmic-ray components by means of a calorimeter in the PAMELA satellite-borne experiment for the case of particle detection within a large aperture. Phys. At. Nucl. 76 (6), 737–747.

Menn, W., Adriani, O., Barbarino, G.C., et al., 2013. The PAMELA space experiment. Adv. Space Res. 51, 209–218.

Stozhkov, Y.I., Basili, A., Bencardino, R., et al., 2005. About separation of hadron and electromagnetic cascades in the PAMELA calorimeter. Int. J. Mod. Phys. A 20 (29), 6745–6748.